AGU PUBLICATIONS

Geophysical Research Letters

RESEARCH LETTER
10.1002/2016GL070002

Key Points:
- Tsunami computations are used to test a tsunami earthquake scenario for the 2015 Chile earthquake
- Any tsunami earthquake slip must be limited to the north of the main shock hypocenter
- A tsunami earthquake is not required to match the tsunami recordings, barring major model trade-offs

Supporting Information:
- Supporting Information S1
- Movie S1
- Movie S2

Correspondence to:
T. Lay,
tlay@ucsc.edu

Citation:
Lay, T., L. Li, and K. F. Cheung (2016), Modeling tsunami observations to evaluate a proposed late tsunami earthquake stage for the 16 September 2015 Illapel, Chile, M_w 8.3 earthquake, *Geophys. Res. Lett.*, *43*, 7902–7912, doi:10.1002/2016GL070002.

Received 14 JUN 2016
Accepted 16 JUL 2016
Accepted article online 20 JUL 2016
Published online 3 AUG 2016

Modeling tsunami observations to evaluate a proposed late tsunami earthquake stage for the 16 September 2015 Illapel, Chile, M_w 8.3 earthquake

Thorne Lay[1], Linyan Li[2], and Kwok Fai Cheung[2]

[1]Department of Earth and Planetary Sciences, University of California, Santa Cruz, California, USA, [2]Department of Ocean and Resources Engineering, University of Hawai'i at Mānoa, Honolulu, Hawaii, USA

Abstract Resolving seaward extent of slip during great subduction zone interplate ruptures using land-based seismological and geodetic observations is challenging. Modeling of tsunami recordings from ocean-bottom pressure sensors of the Deep-ocean Assessment and Reporting of Tsunami (DART) network has added valuable constraints on near-trench slip for recent events. We use DART and tide gauge recordings to evaluate a proposed seismological scenario involving a late M_w 8.08 tsunami earthquake following the ~95 s long main rupture stage of the 16 September 2015 Illapel, Chile, M_w 8.3 earthquake. Tsunami observations constrain the spatial extent of any late tsunami earthquake slip to locate north of the main shock hypocenter. The proposed late shallow slip predicts tsunami signals with considerable amplitudes but shorter wavelengths compared to those of the main stage slip constrained by joint seismic and tsunami modeling, yielding overprediction of first-arrival amplitudes at DART and tide gauge stations when the two stages are combined.

1. Introduction

The shallow portion of subduction zone megathrust faults near the toe of the sedimentary wedge was long thought to be largely aseismic, even in regions where the deeper portion of the fault experiences repeated great earthquake slip events [see *Lay and Bilek*, 2007]. This perspective has changed with the recognition of tsunamigenic rupture of the shallow megathrust either as part of great megathrust-spanning earthquakes like the 2011 Tohoku M_w 9.0 earthquake [e.g., *Lay et al.*, 2011a; *Yamazaki et al.*, 2011b; *Yokota et al.*, 2011] or as isolated shallow ruptures called tsunami earthquakes due to their strong tsunami excitation relative to their surface wave magnitudes [e.g., *Kanamori*, 1972; *Kanamori and Kikuchi*, 1993; *Johnson and Satake*, 1997; *Tanioka and Satake*, 1996a; *Ammon et al.*, 2006; *Lay et al.*, 2011b; *Yue et al.*, 2014a]. Many regions may experience such events, and this places extra emphasis on establishing the updip rupture extent of the more common great megathrust earthquakes to evaluate hazards posed by further tsunamigenic events produced by near-trench rupture.

It is now well recognized that the far-offshore coseismic slip distribution for great subduction zone events is poorly resolved by land-based geodetic and seismic observations. The same is true for most models of interseismic slip deficit or seismic coupling based on coastal geodetic measurements. While future development of seafloor geodesy may overcome this limitation, analysis of tsunami recordings from seafloor pressure sensors of the Deep-ocean Assessment and Reporting of Tsunami (DART) network either alone or in conjunction with tide gauge, seismic, and geodetic observations provides improved constraints on the updip extent of coseismic slip in great earthquakes [e.g., *Lay et al.*, 2011c; *Saito et al.*, 2011; *Yamazaki et al.*, 2011b, 2013; *Satake et al.*, 2013; *An et al.*, 2014; *Yue et al.*, 2014a; *Li et al.*, 2016; *Heidarzadeh et al.*, 2016]. Some events are well resolved to not have coseismic slip extend to near the trench [e.g., *An et al.*, 2014; *Bai et al.*, 2014], while others have localized portions of the rupture zone where coseismic slip does extend to the trench [e.g., *Yue et al.*, 2014b; *Melgar et al.*, 2016; *Yoshimoto et al.*, 2016]. For many other great events, especially older ones, the updip extent of coseismic slip is very poorly understood.

The 16 September 2015 Illapel, Chile, M_w 8.3 megathrust earthquake has been extensively studied using seismic, geodetic, and tsunami data sets, and the rupture has been consistently characterized to involve a large-slip patch offshore extending from about 30°S to 31.6°S, with a secondary slip patch downdip below the coast [e.g., *Heidarzadeh et al.*, 2016; *Li et al.*, 2016; *Ye et al.*, 2016; *Yin et al.*, 2016]. The rupture has at least a 95 s duration and a seismic moment of about 3.2×10^{21} Nm from long-period seismic wave inversions [e.g., *United*

States Geological Survey National Earthquake Information Center (*USGS-NEIC):* http://earthquake.usgs.gov/earthquakes/eventpage/us20003k7a#general]. Slip appears to extend to near the trench, with timing of tsunami arrivals at regional DART stations providing the best constraints on the seaward extent of rupture.

Recently, *Lee et al.* [2016] proposed that the rupture process imaged in earlier source studies of the Illapel earthquake resolved only the first of a two-staged rupture. Based on modeling of regional and teleseismic data with Green's functions computed for a 3-D model, they proposed a second stage of rupture commencing 5 to 10 s after the first ended, involving patchy slip in the shallow megathrust extending along strike from 30°S to 32.8°S, persisting from 100 to 250 s after the earthquake origin time, with cumulative seismic moment of 1.66×10^{21} Nm (M_w 8.08). *Lee et al.* [2016] describe this proposed second stage of rupture as a tsunami earthquake, involving significant rerupturing of the shallow region that failed in the first stage along with slow bilateral expansion of the initial rupture zone. The seismic moment of this proposed late tsunami earthquake exceeds that of any isolated tsunami earthquake of the past 50 years. If the model is correct, it would both reaffirm the potential for near-trench slip to be triggered by deeper slip with a small delay as well as raising questions about how often previous studies of great ruptures have missed delayed slip to the trench.

Routine long-period point source moment tensor inversions such as the *W* phase inversion and centroid moment tensor inversion may fail to detect a low amplitude tail on the moment rate function due to their assumption of a triangular source time function [Hiroo Kanamori, personal communication, 2016]. Inversions that explicitly allow for multiple triangles [e.g., *Duputel et al*., 2012] might be able to constrain a secondary source, but our own *W* phase inversions show typically excellent waveform predictions with a single source [*Ye et al*., 2016], so the effect of any weak secondary source with the same basic location and mechanism must be very subtle. Detailed analysis of long-period moment rate spectra may help bound any contribution from late rupture, but this requires careful seismic processing [E. Okal, personal communication, 2016]. If there is late, rapid (seismogenic) slip of the offshore fault, the process will almost certainly excite tsunami signals. We explore the proposal of a late tsunami earthquake stage using tsunami data to evaluate its viability and to assess the general potential for missing late tsunami earthquake components of great ruptures.

2. Data and Methods: Main Stage Model

The 2015 Illapel tsunami was recorded by azimuthally well distributed, nearby instruments at three DART stations (32402, 32401, 32412), and coastal tide stations north of the source region (Huasco, Coquimbo), south of the source region (Pichidangui, Valparaíso, and Bucalemu) and on an offshore island (Juan Fernandez) (Figure 1a). These, and additional more remote recordings, were modeled by *Li et al.* [2016] and *Heidarzadeh et al.* [2016] in studies of the source process. We use the nearby observations to explore the proposed late tsunami earthquake scenario. The prior tsunami model studies have established that the main stage rupture did not involve significant slip on the megathrust south of about 31.6°S, as any such slip produces too early of tsunami arrivals at the tide stations located to the south. The source slip distributions found in these studies are similar to the main stage rupture in the first 90 to 95 s proposed by *Lee et al.* [2016], other than the latter model having some slip south of 31.6°S that violates the tide gauge observations (which they did not model). In this analysis, we thus do not use the main stage model of *Lee et al.* [2016] but instead use an updated main stage model inverted from teleseismic body waves that does not violate the observed tsunami arrival times.

We invert the same teleseismic data set used by *Li et al.* [2016], comprised of 60 *P* wave and 42 *SH* wave ground displacements filtered in the 0.005–0.9 Hz passband. The inversion method is also the same kinematic multitime window, least squares procedure for a specified fault geometry and rupture velocity [e.g., *Hartzell and Heaton*, 1983; *Kikuchi and Kanamori*, 1992]. We use a slightly modified source grid and along dip varying 1-D Green's functions with variable water depth rather than a uniform 1-D model as in the previous work. The updated fault model extends all the way to the trench (adding one more shallow row to the model of *Li et al.* [2016]) to correspond spatially to the dimensions of the tsunami earthquake model of *Lee et al.* [2016]. The shallowest three rows of our updated model are somewhat deeper (relative to the sea surface) and have shallower dip than the model in *Li et al.* [2016], but the deeper structure is unchanged and was originally simplified from *Hayes et al.* [2012]. Allowing for variable water depth approximately accounts for the basic 2-D structural variations from the trench to land, mainly manifested in strong *P* wave water reverberations generated near the trench.

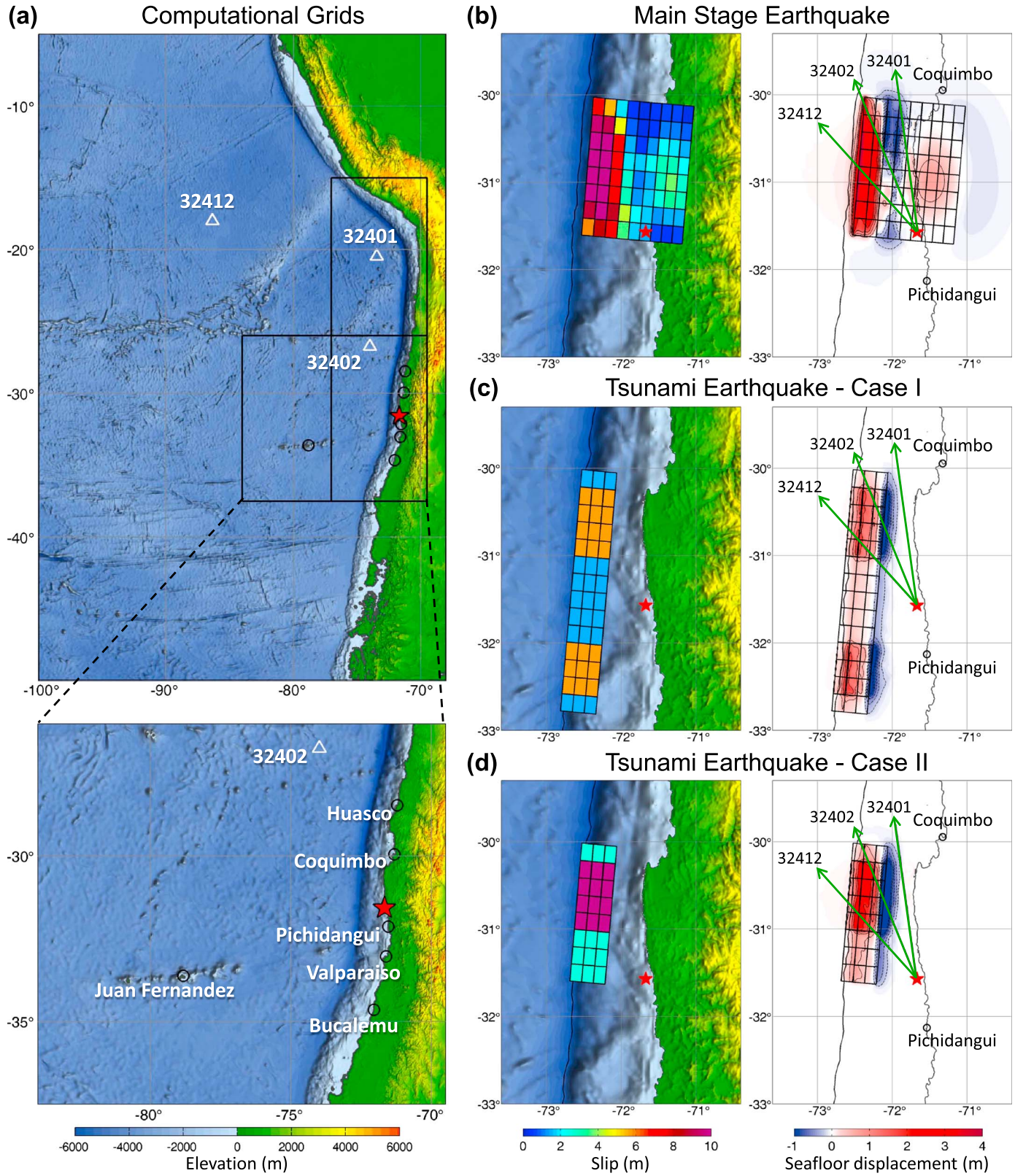

Figure 1. (a) Nested grids used in computing tsunami signals at DART and tide gauge stations. (b) Slip distribution and corresponding uplift and subsidence for the main stage with directions to DART stations indicated. (c) Case I: bilateral patchy slip, uplift, and subsidence for a late-stage tsunami earthquake with total moment equal to that proposed by *Lee et al.* [2016], and (d) Case II: unilateral northward slip of a late-stage tsunami earthquake with total moment equal to that proposed by *Lee et al.* [2016].

As in *Li et al.* [2016], we use the tsunami code NEOWAVE of *Yamazaki et al.* [2009, 2011a] for forward modeling. This staggered finite difference code builds on the nonlinear shallow-water equations with a vertical velocity term to account for weakly dispersive waves and a moment conservation scheme to describe bore formation. The vertical velocity terms also account for the time variation of the seafloor vertical motions prescribed by the slip model through the half-space solution of *Okada* [1985] and facilitate dispersion of the seafloor excitation over the water column during tsunami generation. The method of *Tanioka and Satake* [1996b] approximates the vertical motion contribution from seafloor horizontal displacement on a slope. We use the same nested grids at 2 and 0.5 arc min resolution described by *Li et al.* [2016] for modeling the regional DART and local tide gauge data (Figure 1a). Detailed bathymetry along the coastline is not available to account for local responses to shelf resonance [e.g., *Yamazaki and Cheung*, 2011], so our focus is on comparing the timing and waveform of the first tsunami arrivals at the tide gauges with the codas used for reference only.

We apply the iterative modeling approach used by *Li et al.* [2016] to determine a new main stage 95 s long rupture model that fits both the teleseismic data and the tsunami observations using the modified source grid (supporting information Figures S1 and S2). The resulting slip distribution is very similar to the preferred model of *Li et al.* [2016], but the seismic moment is somewhat larger, $M_0 = 3.2 \times 10^{21}$ Nm (M_w 8.3), which fortuitously matches the long-period moment tensor values reported by the USGS-NEIC, given that the dip varies in our model. The rupture kinematics are the same as in *Li et al.* [2016], with a rupture speed of 3 km/s over the fault surface deeper than the hypocenter and along strike of the model at shallower depth and with an along-dip speed of 1.5 km/s shallower than the hypocenter. The subfault source time functions are parameterized with seven 3 s risetime triangles with overlapping 3 s offsets, giving 24 s possible total time function durations. The main phase rupture has nine rows of subfaults with 15 km width along dip and eight columns with 22 km length along strike. The additional shallow row of the model was not used in the main stage to keep our final model consistent in parameterization with that of *Li et al.* [2016].

The slip model and seafloor uplift for the main stage rupture are shown in Figure 1b, and the observed and computed tsunami signals are shown in Figure 2. The match of the tsunami timing, amplitude, and waveform for the first arrival at all stations is quite good relative to extensive suites of model comparisons explored in the iterative modeling. The agreement is very similar to those shown by *Li et al.* [2016]. There is significant slip in the shallowest portion of the model, and slip to the trench in the main stage is quite plausible. Direct inversions of just the tsunami signals achieve comparable fits [*Heidarzadeh et al*., 2016], and similar slip distribution, but it should be recognized that our model is explicitly an inversion of teleseismic data, with adjustment of otherwise poorly constrained kinematic parameters to match the tsunami observations.

3. Tsunami Earthquake Scenarios

As we want to explore the general possibility of a second stage tsunami earthquake rupture rather than test a single specific model, we produce a suite of simplified slip scenarios constrained by the basic seismic moment, timing, and spatial distribution of the model proposed by *Lee et al.* [2016]. The important parameters for the tsunami earthquake stage are the proposed total moment of 1.66×10^{21} Nm, time of faulting from 100 to 250 s after the origin time, and placement along the uppermost 30 to 45 km of the megathrust, with outcrop at the trench.

We consider a total of eight scenarios, four of which involve bilateral ruptures with 14 columns along strike and the hypocenter near the midpoint, and four of which involve unilateral northward ruptures with eight columns matching the length of the main stage. Uniform slip is distributed along dip over either two or three rows extending to the trench. The bilateral and unilateral models respectively include two asperities and one asperity with four times as much slip as adjacent regions. We use an average rigidity of 3.3×10^{10} N/m^2 to distribute slip over the models such that the total moment is maintained. This rigidity is consistent with the average value derived from the local seismic velocity model used in the seismic wave inversion. As an example, for uniform slip over 45 km width (three rows of subfaults along dip) in the bilateral model, the average slip is 3.62 m. For the single asperity 88 km long in a unilateral model with 30 km width (two rows of subfaults along dip) the slip is 15.2 m in the asperity and 3.80 m outside of it. The risetime of the tsunami earthquake slip functions is distributed from 100 to 250 s, as an approximation of the bursty, prolonged slip during this time interval in the model of *Lee et al.* [2016]. We note that assumption of a lower rigidity will increase the slip estimate

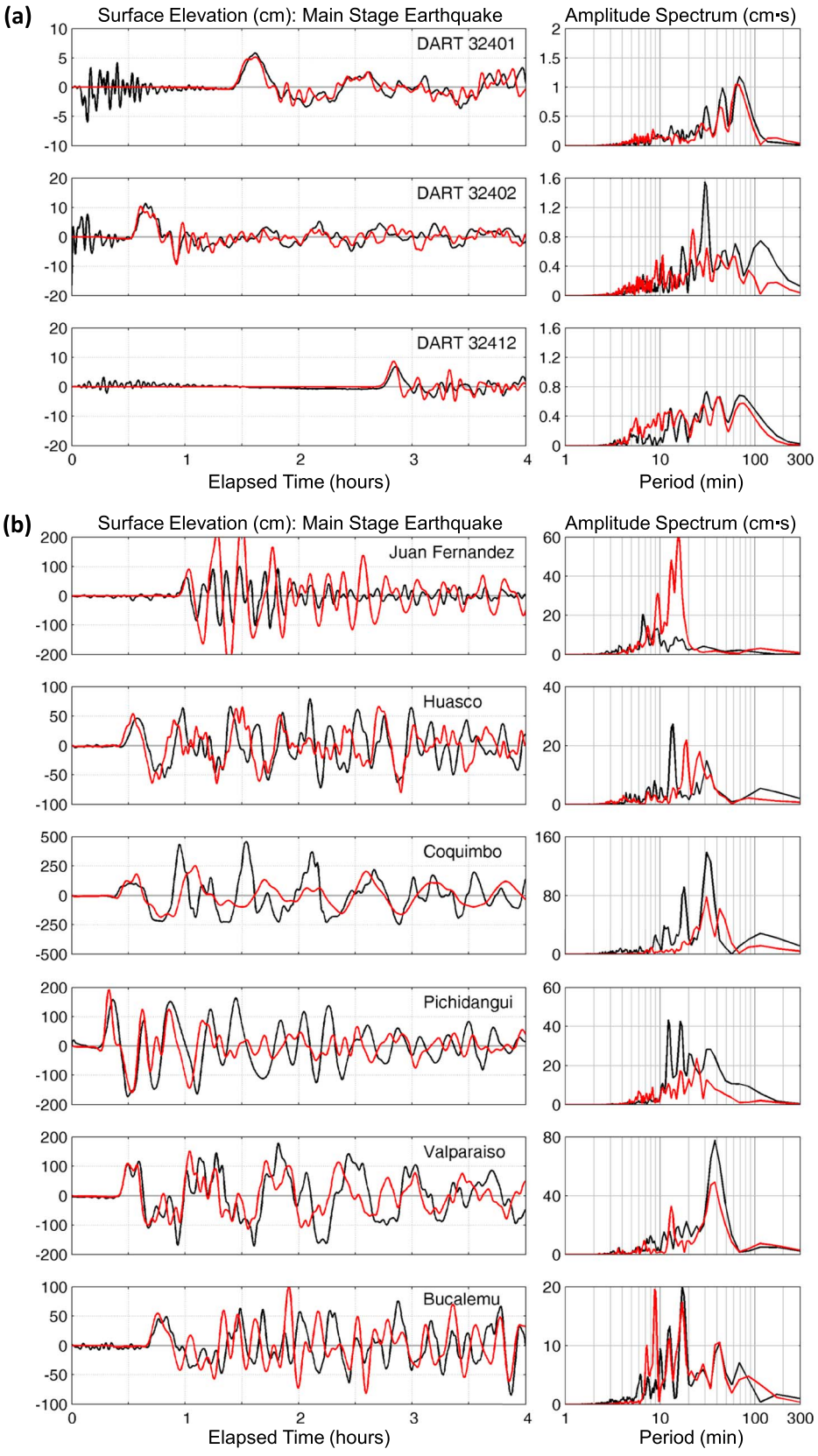

Figure 2. Comparison of observed tsunami waveforms and spectra (black lines) with computations (red lines) for the main stage model in Figure 1b. (a) Regional DART stations. (b) Local tide gauges.

for a given seismic moment, and this can only enhance the tsunami excitation but doing so should be accompanied by reinverting the main phase rupture using a correspondingly adjusted source velocity model in order to determine the effect on the shallow seismic moment distribution. We do not have independent constraints on the detailed shallow rigidity so this is not explored, but we do not expect it would modify any of the findings below.

Figure 1 shows two models for the tsunami earthquake stage, both with 45 km width and nonuniform slip along strike. Case I (Figure 1c) is a bilateral model with two asperities of 5.79 m slip and adjacent regions having 1.45 m slip. This model, with slip activated from 100 to 250 s after the origin time, is a first-order approximation of the tsunami stage model of *Lee et al.* [2016] in terms of slip distribution and total moment. Case II (Figure 1d) is a unilateral model involving a single asperity with slip of 10.1 m surround by slip of 2.5 m.

Figure 3 compares the observations with the computed tsunami signals from the combined main and Case I tsunami earthquake stages and just the tsunami earthquake stage for reference. To address any possible nonlinearity of the tsunami near the coastal tide gauges, we computed the total signals from a single combined slip model rather than linearly superimposing the separate contributions. Relative to the comparisons for just the main stage signal in Figure 2, the predicted waveforms show distinct early arrivals at the Valparaíso and Bucalemu tide gauges, well ahead of the impulsive observed first arrivals. This is similar to what is found for main stage slip models that extend south of the hypocenter. The 100 s delay of onset of the tsunami earthquake signals is far too small to avoid producing these early arrivals. This holds for the other bilateral uniform slip and 30 km wide nonuniform slip models (Figures S3–S6), and we consider this to be a strong constraint on any late tsunami earthquake process within a few minutes after the main shock: slip cannot occur south of the hypocenter. It should be recognized that as long as reasonably good bathymetry is available, the timing of tsunami provides very strong constraints on the spatial extent of seafloor deformation above thrust faults even for prolonged source processes. Overprediction of the initial arrival amplitudes at the DART and tide gauge stations as seen in Figure 3 is also a failing of this tsunami earthquake scenario, but the timing mismatch is most compelling with respect to bounding possible tsunami earthquake occurrence in this case.

Figure 4 shows the waveform comparison for the two-staged event with Case II, in which the unilateral nonuniform slip tsunami earthquake model is constrained northward of the hypocenter. The early arrivals at Valparaíso and Bucalemu and the overprediction at Pichidangui are eliminated. The impulsive arrivals and first cycle waveforms are now reasonably well matched at the three southern tide gauge stations. The issue for this model, along with those involving the uniform slip and 30 km wide versions of unilateral ruptures (Figures S7–S10), is that the late, large shallow slip produces substantial amplitude of the first arrivals at the DART stations and the tide gauges north of the epicenter. The relatively short period signals superimpose on the longer period signals from the broader main stage rupture resulting in overpredictions of all northern tsunami observations. Given that the main stage itself produces good matches to the signals as seen in Figure 2, this is not surprising.

At face value, the discrepancy in the computed and recorded waveform and amplitude and the azimuthal distribution of the mismatches would rule out slip comparable to the proposed M_w 8.08 tsunami earthquake, if the main stage model based on teleseismic inversions is reasonably well defined. Of course, there may be biases in this evaluation due to nonuniqueness in the seismic inversion and the iterative process of adjusting kinematic parameters (fault length, rupture speed) to match the observed tsunami signals assuming they were entirely generated by the main stage rupture. While it is safe to say that a late-stage tsunami earthquake is not needed to match the tsunami data, it is harder to say how much late-stage tsunami earthquake could be tolerated by the observations. If the seismic model is forced to slip only on the deeper portion of the megathrust, or with less updip slip, the initial main stage signals at the DART stations could be reduced, allowing improvement of the fit to the records when augmented by late-stage arrivals from the shallow slip. Simultaneous reduction of the amplitude of the signals and avoiding early arrivals at the northern tide gauges would also have to be achieved. Such modeling is ill-posed so we do not attempt to bound viable solutions, other than to note that our main stage model already has lower moment than that of *Lee et al.* [2016]. We believe it is at least possible to reject the hypothesis that there has to have been late tsunami earthquake contributions for this event. This perspective is reinforced by inversions of the tsunami data alone by *Heidarzadeh et al.* [2016], who allowed for very low rupture velocity models with source durations longer than 100 s, finding that slip was placed very shallow near the trench (in their supporting information). Such

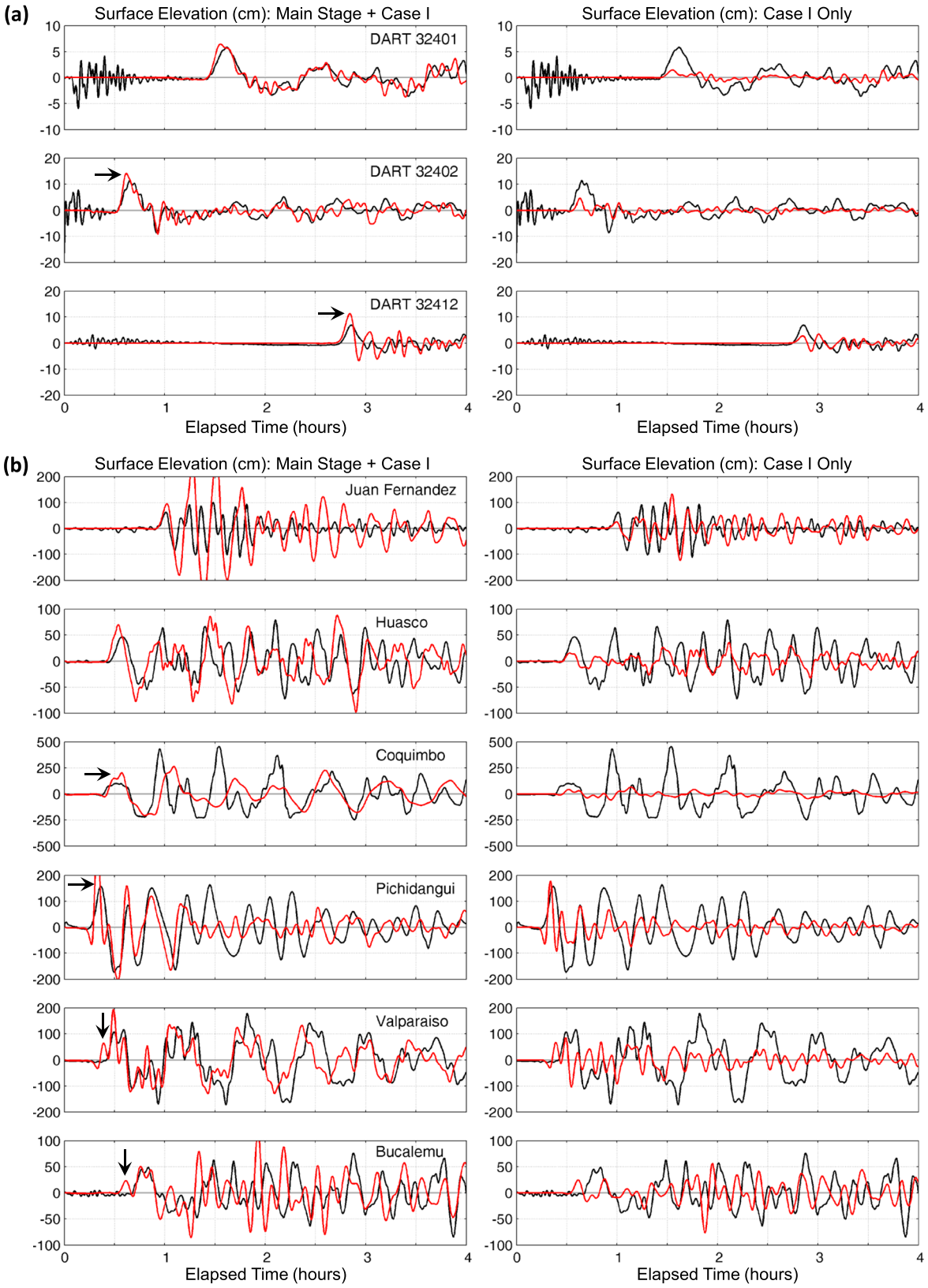

Figure 3. Comparison of tsunami observations (black lines) with computed tsunami waveforms (red lines) from the main stage (Figure 1b) plus Case I bilateral tsunami earthquake model (Figure 1c) combined on the left and for just the tsunami earthquake stage on the right. (a) Regional DART stations. (b) Local tide gauges. Horizontal arrowheads indicate amplitude mismatches and vertical arrowheads indicate timing mismatches.

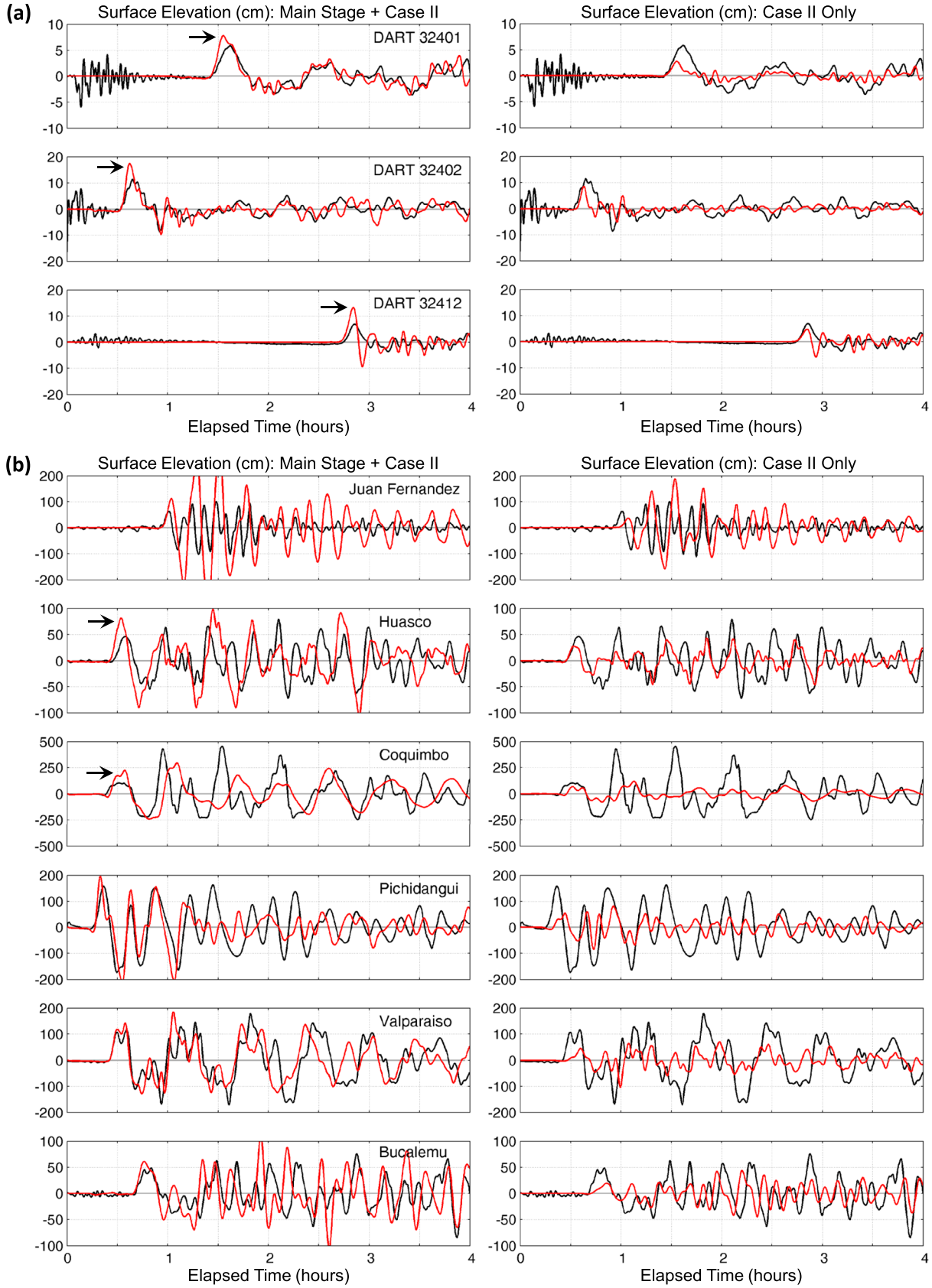

Figure 4. Similar to Figure 3 for the Case II unilateral tsunami earthquake model (Figure 1d).

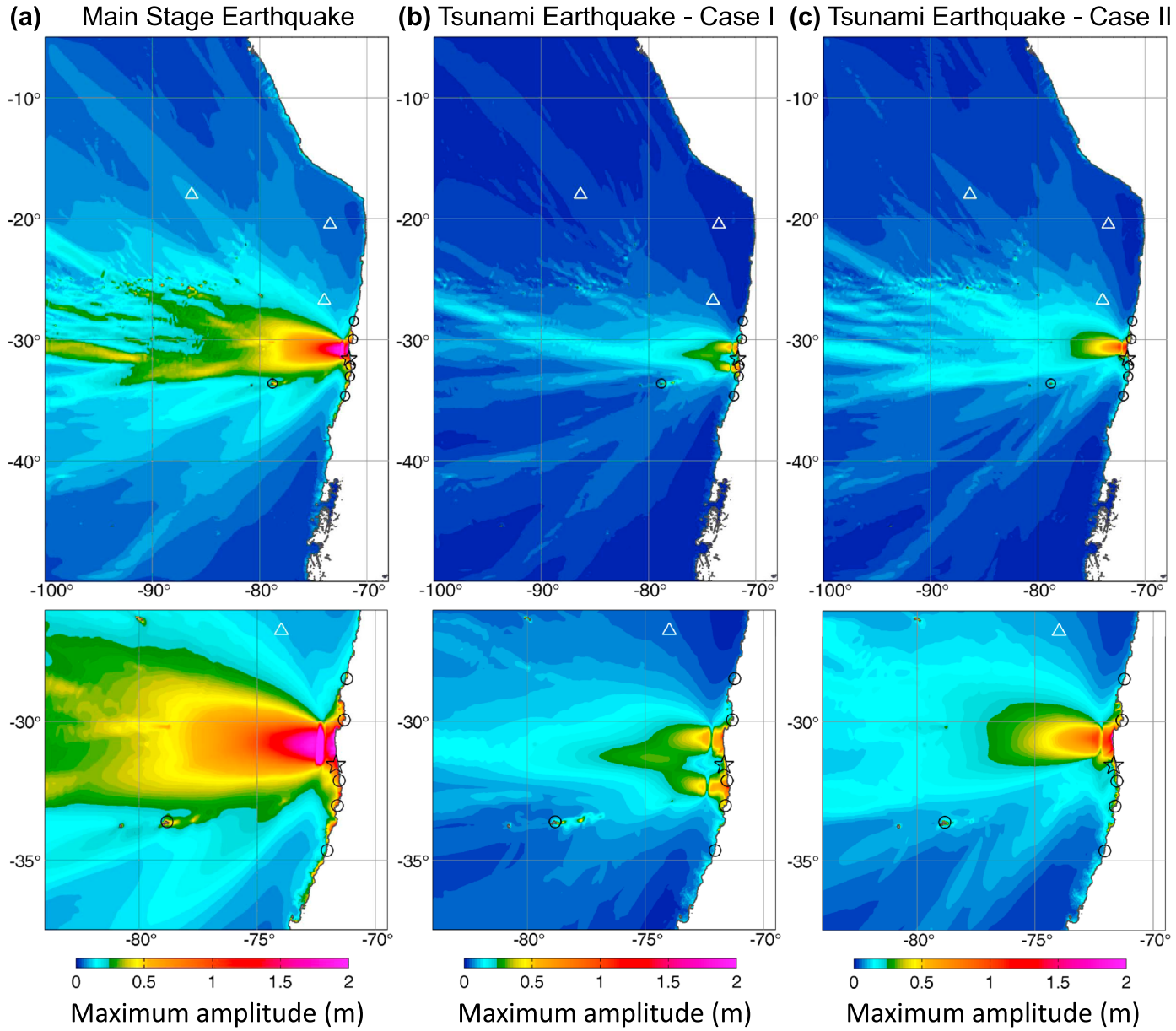

Figure 5. Maps showing the peak sea surface amplitudes. (a) Main stage rupture. (b) Case I tsunami earthquake rupture. (c) Case II tsunami earthquake model (right). The DART stations (triangles) and coastal tide gauge stations (circles) are oblique to the primary tsunami radiation.

models did not fit the tsunami data well, and they also conclude that bilateral slip models do not fit southern tsunami observations, as found here and by *Li et al.* [2016].

4. Discussion and Conclusions

Figure 5 shows the sea level predictions for the models in Figure 1, clarifying that maximum tsunami signals are located directly seaward from the coast and on the coast along the slip zone. Unfortunately, the DART stations are rather obliquely located relative to the main radiation. Movies S1 (Case I) and S2 (Case II) in the supporting information show the initial signals from the main stage, and tsunami earthquake ruptures are well aligned in the near and far field despite the time lag. The waves from the two stages reach the shore at nearly the same time but excite different sets of oscillation modes associated with their dominant periods. Recorded peak runup values have no time histories but provide an additional dataset to test for the

possibility of late tsunami earthquake occurrence. However, high-resolution coastal bathymetry and topography will be needed to model the local runup observations [e.g., *Aránguiz et al*., 2015].

The use of 3-D Green's functions to improve finite-source inversions is a state-of-the-art endeavor, and it likely represents the future standard. However, current models lack detailed structures near subduction zone trenches. *Lee et al.* [2016] show that there are late reverberative *P* wave coda arrivals at large distances (such that PP is not in the time window), and these are clearly present (Figure S2). However, even with our simplified local 1-D structure Green's functions, we account for most of these oscillations by prolonged water reverberations generated by slip during the main stage rupture. This is further demonstrated by finite-fault inversion of just *P* waves from epicentral distances greater than 65°, which gives a model (Figure S11) very consistent with our main stage rupture model, for which extended calculation of the coda matches the *P* signals from 100 to 200 s quite well, except at stations east and west of the source where the amplitudes are underpredicted (Figure S12). As this *P* coda signal plays a significant role in Lee et al.'s argument for a late tsunami stage, this calculation suggests that they overestimate the strength of any late tsunami earthquake. Significant reduction (or elimination) of its moment would improve the match to the tsunami signals for the scenarios that we consider. It remains difficult to resolve the timing and distribution of very shallow megathrust slip with only seismic wave inversion.

Acknowledgments

The IRIS DMS data center (http://www.iris.edu/hq/) was used to access the seismic data from Global Seismic Network and Federation of Digital Seismic Network stations. The DART and tide gauge data were downloaded from the NOAA National Data Buoy Center (http://www.ndbc.noaa.gov/) and CO-OPS Tsunami Capable Tide Stations (http://tidesandcurrents.noaa.gov/tsunami/). H. Kanamori provided information about W phase inversion for the model with late tsunami earthquake. E. Okal provided preliminary information about the long-period moment estimates for the event. We thank two anonymous reviewers for helpful suggestions. This data analysis made use of GMT, SAC, and MATLAB software. This work was supported by NOAA grant NA15NWS4670025 to Kwok Fai Cheung and by NSF grant EAR1245717 to Thorne Lay. SOEST contribution 9676.

References

Ammon, C. J., H. Kanamori, T. Lay, and A. A. Velasco (2006), The 17 July 2006 Java tsunami earthquake, *Geophys. Res. Lett.*, *33*, L234308, doi:10.1029/2006GL028005.

An, C., I. Sepúlveda, and P. L.-F. Liu (2014), Tsunami source and its validation of the 2014 Iquique, Chile earthquake, *Geophys. Res. Lett.*, *41*, 3988–3994, doi:10.1002/2014GL060567.

Aránguiz, R., et al. (2015), The 16 September 2015 Chile tsunami from the post-tsunami survey and numerical modeling perspectives, *Pure Appl. Geophys.*, *321*(2), 333–348, doi:10.1007/s00024-015-1225-4.

Bai, Y., K. F. Cheung, Y. Yamazaki, T. Lay, and L. Ye (2014), Tsunami surges around the Hawaiian Islands from the 1 April 2014 North Chile M_W 8.1 earthquake, *Geophys. Res. Lett.*, *41*, 8512–8521, doi:10.1002/2014GL061686.

Duputel, Z., H. Kanamori, V. C. Tsai, L. Rivera, L. Meng, J.-P. Ampuero, and J. M. Stock (2012), The 2012 Sumatra great earthquake sequence, *Earth Planet. Sci. Lett.*, *351–352*, 247–257.

Hartzell, S. H., and T. H. Heaton (1983), Inversion of strong ground motion and teleseismic waveform data for the fault rupture history of the 1979 Imperial Valley, California, earthquake, *Bull. Seismol. Soc. Am.*, *73*(6A), 1553–1583.

Hayes, G. P., D. J. Wald, and R. L. Johnson (2012), Slab1.0: A three-dimensional model of global subduction zone geometries, *J. Geophys. Res.*, *117*, B01302, doi:10.1029/2011JB008524.

Heidarzadeh, M., S. Murotani, K. Satake, T. Ishibe, and A. R. Gusman (2016), Source model of the 16 September 2015 Illapel, Chile, M_W 8.4 earthquake based on teleseismic and tsunami data, *Geophys. Res. Lett.*, *43*, 643–650, doi:10.1002/2015GL067297.

Johnson, J. M., and K. Satake (1997), Estimation of seismic moment and slip distribution of the April 1, 1946, Aleutian tsunami earthquake, *J. Geophys. Res.*, *102*, 11,765–11,779, doi:10.1029/97JB00274.

Kanamori, H. (1972), Mechanism of tsunami earthquakes, *Phys. Earth Planet. Int.*, *6*, 246–259.

Kanamori, H., and M. Kikuchi (1993), The 1992 Nicaragua earthquake: A slow tsunami earthquake associated with subducted sediments, *Nature*, *361*, 714–716.

Kikuchi, M., and H. Kanamori (1992), Inversion of complex body waves—III, *Bull. Seismol. Soc. Am.*, *81*(6), 2335–2350.

Lay, T., and S. L. Bilek (2007), Anomalous earthquake ruptures at shallow depths on subduction zone megathrusts, in *The Seismogenic Zone of Subduction Thrust Faults*, edited by T. H. Dixon and J. C. Moore, pp. 476–511, Columbia Univ. Press, New York.

Lay, T., C. J. Ammon, H. Kanamori, L. Xue, and M. J. Kim (2011a), Possible large near-trench slip during the 2011 M_w 9.0 off the Pacific coast of Tohoku Earthquake, *Earth Planets Space*, *63*(7), 687–692, doi:10.5047/eps.2011.05.033.

Lay, T., C. J. Ammon, H. Kanamori, Y. Yamazaki, K. F. Cheung, and A. Hutko (2011b), The 25 October 2010 Mentawai tsunami earthquake (M_w 7.8) and the tsunami hazard presented by shallow megathrust ruptures, *Geophys. Res. Lett.*, *38*, L13301, doi:10.1029/2010GL046552.

Lay, T., Y. Yamazaki, C. J. Ammon, K. F. Cheung, and H. Kanamori (2011c), The 2011 M_w 9.0 off the Pacific coast of Tohoku Earthquake: Comparison of deep-water tsunami signals with finite-fault rupture model predictions, *Earth Planets Space*, *63*(7), 797–801, doi:10.5047/eps.2011.05.030.

Lee, S.-J., T.-Y. Yeh, T.-C. Lin, Y.-Y. Lin, T.-R. Alex Song, and B.-S. Huang (2016), Two-stage composite megathrust rupture of the 2015 M_W8.4 Illapel, Chile earthquake identified by spectral-element inversion of teleseismic waves, *Geophys. Res. Lett.*, *43*, 4979–4985, doi:10.1002/2016GL068843.

Li, L., T. Lay, K. F. Cheung, and L. Ye (2016), Joint modeling of teleseismic and tsunami wave observations to constrain the 16 September 2015, Illapel, Chile, M_W 8.3 earthquake rupture process, *Geophys. Res. Lett.*, *43*, 4303–4312, doi:10.1002/2016GL068674.

Melgar, D., W. Fan, S. Riquelme, J. Geng, C. Liang, M. Fuentes, G. Vargas, R. M. Allen, P. M. Shearer, and E. J. Fielding (2016), Slip segmentation and slow rupture to the trench during the 2015, M_W 8.3 Illapel, Chile earthquake, *Geophys. Res. Lett.*, *43*, 961–966, doi:10.1002/2015GL067369.

Okada, Y. (1985), Surface deformation due to shear and tensile faults in a half space, *Bull. Seism. Soc. Am.*, *75*(4), 1135–1154.

Saito, T., Y. Ito, D. Inazu, and R. Hino (2011), Tsunami source of the 2011 Tohoku-Oki earthquake, Japan: Inversion analysis based on dispersive tsunami simulations, *Geophys. Res. Lett.*, *38*, L00G19, doi:10.1029/2011GL049089.

Satake, K., Y. Nishimura, P. S. Putra, A. R. Gusman, H. Sunendar, Y. Fujii, Y. Tanioka, H. Latief, and E. Yulianto (2013), Tsunami source of the 2010 Mentawai, Indonesia earthquake inferred from tsunami field survey and waveform modeling, *Pure Appl. Geophys.*, *170*(9), 1567–1582, doi:10.1007/s00024-012-0536-y.

Tanioka, Y., and K. Satake (1996a), Fault parameters of the 1896 Sanriku tsunami earthquake estimated from tsunami numerical modeling, *Geophys. Res. Lett.*, *23*, 1549–1552, doi:10.1029/96GL01479.

Tanioka, Y., and K. Satake (1996b), Tsunami generation by horizontal displacement of ocean bottom, *Geophys. Res. Lett.*, *23*, 861–864, doi:10.1029/96GL00736.

Yamazaki, Y., and K. F. Cheung (2011), Shelf resonance and impact of near-field tsunami generated by the 2010 Chile earthquake, *Geophys. Res. Lett.*, *38*, L12605, doi:10.1029/2011GL047508.

Yamazaki, Y., Z. Kowalik, and K. F. Cheung (2009), Depth-integrated, non-hydrostatic model for wave breaking and run-up, *Int. J. Numer. Methods Fluids*, *61*(5), 473–497.

Yamazaki, Y., K. F. Cheung, and Z. Kowalik (2011a), Depth-integrated, non-hydrostatic model with grid nesting for tsunami generation, propagation, and run-up, *Int. J. Numer. Methods Fluids*, *67*(12), 2081–2107.

Yamazaki, Y., T. Lay, K. F. Cheung, H. Yue, and H. Kanamori (2011b), Modeling regional and remote tsunami observations with finite-fault slip models for the 11 March 2011 Tohoku earthquake (M_w 9.0), *Geophys. Res. Lett.*, *38*, L00G15, doi:10.1029/2011GL049130.

Yamazaki, Y., K. F. Cheung, and T. Lay (2013), Generation mechanism and near-field dynamics of the 2011 Tohoku tsunami, *Bull. Seism. Soc. Am.*, *103*, 1444–1455, doi:10.1785/0120120103.

Ye, L., T. Lay, H. Kanamori, and K. D. Koper (2016), Rapidly estimated seismic source parameters for the 16 September 2015 Illapel, Chile M_W 8.3 earthquake, *Pure Appl. Geophys.*, *321*(2), 321–332, doi:10.1007/s00024-015-1202-y.

Yin, J., H. Yang, H. Yao, and H. Weng (2016), Coseismic radiation and stress drop during the 2015 M_W 8.3 Illapel, Chile megathrust earthquake, *Geophys. Res. Lett.*, *43*, 1520–1528, doi:10.1002/2015GL067381.

Yokota, Y., K. Koketsu, Y. Fujii, K. Satake, S. Sakai, M. Shinohara, and T. Kanazawa (2011), Joint inversion of strong motion, teleseismic, geodetic and tsunami datasets for the rupture process of the 2011 Tohoku earthquake, *Geophys. Res. Lett.*, *38*, L00G21, doi:10.1029/2011GL050098.

Yoshimoto, M., S. Watada, Y. Fujii, and K. Satake (2016), Source estimate and tsunami forecase from far-field deep-ocean tsunami waveforms—The 27 February 2010 M_W 8.8 Maule earthquake, *Geophys. Res. Lett.*, *43*, 659–665, doi:10.1002/2015GL067181.

Yue, H., T. Lay, L. Rivera, Y. Bai, Y. Yamazaki, K. F. Cheung, E. M. Hill, K. Sieh, W. Kongko, and A. Muhari (2014a), Rupture process of the 2010 M_w 7.8 Mentawai tsunami earthquake from joint inversion of near-field hr-GPS and teleseismic body wave recordings constrained by tsunami observations, *J. Geophys. Res. Solid Earth*, *119*, 5574–5593, doi:10.1002/2014JB011082.

Yue, H., T. Lay, L. Rivera, C. An, C. Vigny, X. Tong, and J. C. Báez Soto (2014b), Localized fault slip to the trench in the 2010 Maule, Chile M_w 8.8 earthquake from joint inversion of high-rate GPS, teleseismic body waves, InSAR, campaign GPS, and tsunami observations, *J. Geophys. Res. Solid Earth*, *119*, 7786–7804, doi:10.1002/2014JB011340.